BLOSM

Boron-based large-scale observation of soil moisture: First laboratory results of a cost-efficient neutron detector

van Amelrooij, Edward; van de Giesen, Nick; Plomp, Jeroen; Thijs, Michel; Fico, Tomáš

Important note
To cite this publication, please use the final published version (if applicable).
Please check the document version above.

BLOSM: Boron-based large-scale observation of soil moisture: First laboratory results of a cost-efficient neutron detector

Edward van Amelrooij [a], Nick van de Giesen [a,*], Jeroen Plomp [b], Michel Thijs [b], Tomáš Fico [c]

[a] Department of Water Management, Faculty of Civil Engineering & Geosciences, Delft University of Technology, 2628 CN Delft, The Netherlands
[b] Reactor Institute Delft, Delft University of Technology, 2628 CN Delft, The Netherlands
[c] MicroStep-MIS, spol. s r.o., 831 04 Bratislava, Slovakia

ARTICLE INFO

Article history:

Keywords:
Neutrons
Soil-moisture
CRNS
Boron
ZnS
Wavelength shifting fibers

ABSTRACT

A newly developed Boron-based Large-scale Observation of Soil Moisture (or BLOSM) system is currently being tested and implemented. The stationary system provides a cost-effective way to measure fast and thermalized neutrons by using low-cost, non–hazardous and accessible materials and equipment. BLOSM operates by measuring cosmic-ray induced neutrons and by comparing the amount of fast neutrons with the amount of thermal neutrons. Fast neutrons are moderated by hydrogen atoms in the air, organic materials, and especially and primarily by water in the soil, causing the ratio between fast and thermal to be a strong indicator of soil moisture content. The fast/thermal ratio is representative for soil moisture a scale of about 30 hectares, while standard soil moisture measurements are representative for less than a square meter. This is a well-established fact but present neutron detectors are very costly. Thanks to the low-cost of the probe, BLOSM can eventually be applied at a large scale and significantly increase the number of soil–water data points thereby enabling improvement of existing hydrology models as well as new applications such as monitoring fire hazards and agricultural droughts. Here, we present the build and first tests in the laboratory. We show that BLOSM can indeed measure fast and thermal neutrons, which opens the way to applications outside the laboratory.

© 2022 The Author(s). Published by Elsevier Ltd. This is an open access article under the CC BY-NC-ND license (http://creativecommons.org/licenses/by-nc-nd/4.0/).

Specifications table

Hardware name	BLOSM: Boron-based Large-scale Observation of Soil Moisture
Subject Area	Environmental, planetary and agricultural sciences
Hardware type	Field measurements and sensors
Closest commercial analog	The COsmic-ray Soil Moisture Observing System (COSMOS).https://cosmos.ceh.ac.uk/
Open source license	CERN Open Hardware License (OHL)
Cost of hardware	<$1000
Source file repository	https://dx.doi.org/10.17605/osf.io/jgrm8

1. Hardware in context

Soil moisture content is a critical part of hydrological models used to optimise water management and agricultural productivity as well as to produce meteorological forecasts and events like floods, agricultural droughts and forest fires. Standard soil moisture probes are only valid at very small scales of a few decimetres. Soil-moisture measurements at hectometre scale are a missing link in the calibration of hydrological models and satellite measurements, which are typically at scales from tens to thousands of metres. Ideally, a large number of large-scale detectors would be installed to provide sufficient soil moisture data-points to significantly improve current hydrological models.

Our atmosphere is continuously bombarded by cosmic rays, each one causing a shower of sub-atomic particles, such as muons, pions, neutrons, protons, and photons, raining down on the Earth's surface [21]. Muon detection low cost was one of the inspirations for the present work [1]. At the Earth's surface, 95% of the particles are neutrons [21]. When just produced, these neutrons travel very fast (15,000 km/s) but while they bounce off nuclei, they loose kinetic energy and come into thermal equilibrium. Thermal equilibrium means that the impulse of the neutrons is more or less equal to the impulse of regular atoms, which implies speeds of about 2 km/s. Different substances have different efficiencies with which they slow down fast neutrons but hydrogen rich substances, such as water, are very good at thermalising neutrons. The wetter the environment, the higher the ratio of thermal to fast neutrons will be. Given the speed of neutrons, this ratio depends on a relatively large footprint with a radius of about 300 m [22]. This relation has been known to exist since the 1960s and is being used operationally by hydrologists also for quite some time [4]. It should be noted that there are no detectors for fast neutrons that can be used in the field. There are detectors that detect thermal neutrons. By enclosing one detector in a moderating medium that is rich in hydrogen, fast neutrons will be slowed down enough to become detectable. In our case, we encase one detector in high-density polyethylene (HDPE).

Detectors using cosmic-ray neutron sensing (CRNS) have shown to be able to acquire these hectometer-scale measurements [22]. However, due to the high costs of current CRNS soil-moisture detectors, installing them in large numbers is problematic [22,18]. The main bottleneck is that these sensors are based on helium-3, which is very expensive and, as a by-product of the storage of nuclear warheads, is becoming ever rarer [8]. Here, we have developed an alternative that is cost-effective and could, once it has been tested in the field, be used to cover large areas.

Before we describe our solution, we need to mention neutron probes that are also used to measure soil moisture [2]. Neutron probes carry a source of fast neutrons, typically a mixture of americium and beryllium. It also has a boron trifluoride thermal neutron detector. The complete probe is lowered into an aluminium tube and, at different depths, the number of thermal neutrons is counted. The wetter the soil, the more fast neutrons will be slowed down and come back to the probe, where they can be detected. When used properly, the neutron probe is very useful but its footprint is still very limited to a few decimetres.

We describe a Boron-based Large-scale Observation of Soil Moisture (BLOSM) system that does not involve present disadvantages for CRNS detectors, like high-costs, use of toxic or enriched materials, and need for advanced electronics. Recent developments in silicon-based photomultipliers are combined with well-known neutron sensitive materials to achieve a low-cost neutron detector. A total expenditure below $1000 for two detectors (thermal and fast) offers the possibility of large-scale implementation while still making use of the advantages of CRNS.

2. Hardware description

There are a number of nuclei that have a large cross-section for thermal neutrons and are, therefore, good at capturing them. Especially helium-3, lithium-6 and boron-10 are good at capturing neutrons. For BLOSM, we chose natural boron nitride (^{nat}BN or BN) as a neutron capture agent and silver-doped zinc sulfide (ZnS:Ag) as a scintillator [11,12]. As opposed to pre-existing CRNS soil moisture detectors, BLOSM does not use toxic, flammable, hygroscopic, high-cost, or enriched materials [22,15,18]. The advantage of using natural boron in comparison to the commonly used enriched isotopes like Boron-10, Lithium-6 or even He-3, is a significantly lower-cost, ease of acquisition, import and export. Only 20% of natural Boron consists of the neutron absorbing Boron-10 isotope [16]. To compensate for this loss of neutron absorbing efficiency in comparison to enriched Boron-10 the sensitive area to capture neutrons has to be relatively large, which is not really a problem for our application. The neutron is captured by a boron-10 nucleus, which, in turn, decays into a lithium-7 and an alpha particle:

$$^{10}_{5}B_{10} + ^{1}_{0}n_{1} \rightarrow ^{4}_{2}He_{4} \ (\alpha) + ^{7}_{3}Li_{7} + 2.38 MeV \tag{1}$$

The Boron-nitride (BN) is mixed with ZnS:Ag, a scintillator with a high light yield when interacting with the alpha radiation released after a Boron-10 atom absorbs a neutron [19]. ZnS:Ag is a well-known scintillator with a slow response allowing for slower, and therefore, more economical electronics [17,7]. Another advantage of ZnS:Ag is the clear difference in response to a neutron and a gamma which facilitates the Pulse Shape Discrimination (PSD) and makes identifying neutrons easier [17]. When an alpha particle hits a ZnS:Ag particle, typically up to 170,000 blue and UV photons are produced [14].

Both BN and ZnS:Ag are white powders so a binder material is used in order to bind them together. Here Kraton (D1161) is used because it is transparent and easily dissolved in white spirit. This will result in a paint-like substance and can be applied as such. The paint will result in an almost opaque mixture which limits the maximum thickness of the material

at approximately 0.25 mm in order to allow photons to escape the layer [12,11,6]. The paint is applied to a film of reflective foil to reflect photons escaping from the back side and increase light collection.

Whenever a scintillation occurs and the emitted light escapes the layer, the light needs to get to the Silicon Photomultiplier sensor (SiPM) [5]. The light is faint and the SiPM is small (6 mm × 6 mm) so wavelength-shifting fibers are used as a method of light transport. The fibers are placed directly on the paint surface parallel to each other with both ends connected to the SiPM. The scintillation light is absorbed by a fiber with pigments that shift incoming light to light with a lower wavelength that stays inside the fiber core. Due to the smaller angle of total reflection, a portion of this light is trapped in the fiber and will reach the ends of the fiber where it is connected to the SiPM. The cost of a SiPM is significantly lower than a conventional photomultiplier but the sensitive area is limited (6 mm × 6 mm). Fortunately, the small diameter (1 mm) of the wavelength shifting fibers makes it possible to connect 18 fibers to the SiPM with both ends.

Due to the large area needed and the large attenuation length (>3 m) of the WSL fibers [10] the optimal geometry of the sensitive material is in fact a very long strip, or ribbon. This ribbon can be coiled up to decrease the size of the detector. The coiled up ribbon together with the SiPM are positioned in a cylindrical light-tight and air-tight casing made out of aluminium (1 mm wall thickness) for the bare detector or HDPE (2.5 cm wall thickness) for the moderated detector. A general schematic of the set-up is shown in Fig. 1.

The detector is able to detect neutrons as well as gamma radiation. The signal readout can be carried out by a device with an ADC frequency of at least 200 MHz. This allows easy distinction between gamma rays and neutrons using Pulse Shape Discrimination. During the prototype phase of BLOSM, a Picoscope 2204A and a laptop were used for data acquisition and processing, later a custom PCB and a Raspberry Pi (raspberrypi.org) were used to replace both devices. The processing of data is straightforward and will result in a simple count of neutrons and gamma's.

- The ratio of fast and thermal neutrons can be used for large area (∼300 m radius) soil-moisture measurements. This enables the combination of *in situ* measurements with large-scale satellite measurements and increases the accuracy of hydrological models. Here, we show that BLOSM can measure this ratio under laboratory conditions.
- Due to the low-cost (<$1000) the detectors can be produced and deployed in large quantities. This in turn allows for an increase in data points and therefore gives a more accurate representation of the distribution of water on the land surface, once BLOSM can be deployed in the field.
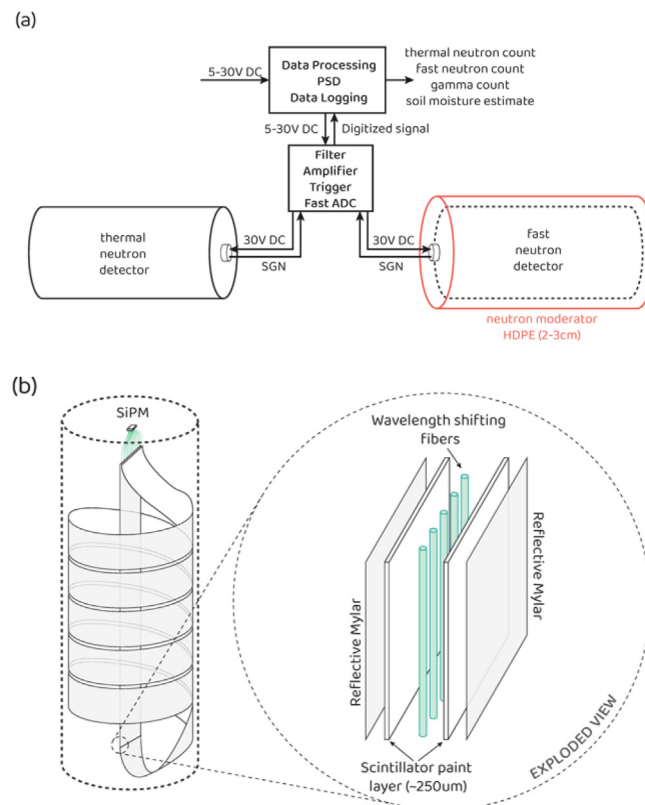

Fig. 1. a) Schematic of the BLOSM setup. A dual-channel PCB is connected directly to the SiPMs in both detectors. This circuit filters, and amplifies the signal after which it can trigger on a pulse to output a digitised signal. Next, a Raspberry Pi receives the digitised signal, applies the Pulse Shape Discrimination (PSD) and outputs the counts and an estimate of the soil moisture content. b) Schematic of the inside of the detectors and the layered structure of the neutron sensitive ribbons.

- Real-time soil-moisture measurements give insight in the hydrological patterns and help us to predict forest fires, floods and droughts, as well as to optimise water use in agricultural areas.
- A single bare detector can be used as an economical thermal neutron detector. In the same way a single moderated detector can be used as an economical epithermal and fast neutron detector.

3. Design files summary

All files can be found in the online repository (https://osf.io/jgrm8/). There are three schematic files (pdf) that show how the different parts of the SiPM module, the ADC module, and the connection with the Raspberry Pi, are connected. These also show how these three parts should be connected. For each part, the Gerber files are provided, which can be used to have the different PCBs produced. The layouts of the PCBs aer also provided as pdf. Finally, there are two Python scripts, one to be used on the Raspberry Pi to collect and store the data from the ADC, and one to be run off-line to analyse the data.

Design filename	File type	Open source license	Location of the file
SiPM PCB layout	PDF	CERN OHL V2	OSF
SiPM PCB	Gerber files (.zip)*	CERN OHL V2	OSF
SiPM module schematic	PDF	CERN OHL V2	OSF
Raspberry Pi (4) IOLe Adaptor Schematic	PDF	CERN OHL V2	OSF
Raspberry Pi (4) IOLe Adaptor PCB	Gerber files (.zip)	CERN OHL V2	OSF
ADC board schematic	PDF	CERN OHL V2	OSF
ADC board PCB	Gerber files (.zip)	CERN OHL V2	OSF
Software ADC board	.hex	CERN OHL V2	OSF
Software Raspberry Pi serial read	Python (.py)	CERN OHL V2	OSF
Software Analyse Data	Python (.py)	CERN OHL V2	OSF

* The SiPM PCB Gerber files are derived from http://www.cosmicwatch.lns.mit.edu/Cosmic Watch muon detector.

4. Bill of materials summary

The quantities in the bill of materials are estimated for a setup consisting of two detectors with a sensitive area of 3100 cm^2. Each detector contains twelve fibers with a length of 2 meter. The fibers are placed at an interval of 7 mm and sandwiched by two scintillator ribbons of 8.4 cm $\times$ 184.5 cm.

Component	Number	Cost per unit	Total cost	Source of materials	Material type
Kraton™D Polymers (SIS) D1161	40g	40€/kg*	1.60€	Kraton Polymers LLC	Polymer
BN: HeBoFill LL-SP 010‡	80g	364€/kg*	29.12€	Ceratec Technical Ceramics BV	Ceramic
Zinc-sulfide silver-doped (ZnS:Ag) ‡	320g	450€/kg	144.00€	WIN-TRUST Technology Co. , LTD	Inorganic
White Spirit	0.5L	5€/L	2.50€	Hardware store	Organic
Poly-vinyl Alcohol (PVA)	10mL	14€/L	0.14€	Polyester shoppen	Polymer
Mylar Reflective Foil	6200 cm^2	4.10/m^2	2.54€	Easygrow	Other
Wavelength Shifting Fiber	48m	5.50€/m*	264.00€	Kuraray Y-11[300]	Polymer
Oscilloscope†	1	129€	129.00€	Picoscope 2204A	Other
Cable gland	4	1.09€	4.36€	Skintop M12 Cable gland	Other
Counter Nut	2	1.52€	3.04€	M12 counter nut	Other
M3/M4 bolts (min. 50 mm)	8	0.25€	2€	Hardware Store	Other
M3/M4 nuts	8	0.10€	0.80€	Hardware Store	Other
3mm plywood (3 cm $\times$ 3 cm)	4	1€	4€	Hardware Store	Other
Aluminium casing ø15cm	40cm	7€/m	2.8€	Hardware Store orSpiro-duct	Other
Aluminium lids ø15 cm	2	4€	8€	Hardware Store orSpiro-lid	Other
HDPE tube (27.4 mm wall thickness)	40 cm	150€/m*	60€	RDM	Other

(continued)

Component	Number	Cost per unit	Total cost	Source of materials	Material type
HDPE sheet 2–3 cm (20 cm × 20 cm)	2	40€	80€	HDPE Sheet	Other
Black isolation tape	1	1€	1€	Hardware Store	Other
Optical Coupling Grease	1	5€	5€	iRad Silicone Coupling Compound	Other

* : Inquiry based orders. Unit price is an indication and can differ due to lower or higher quantity order.

† : The oscilloscope can be replaced with any other ADC as long as it can compute one data point every 200ns for two channels.

‡ : To increase scintillation efficiency the particle size of the BN should be smaller than the ZnS:Ag particles to ensure that the ZnS:Ag is contained in a thin layer of BN. Here particles sizes of ~1 μm and ~7.5 μm are used for BN and ZnS:Ag respectively.

4.1. SiPM surface mount electronic parts

Designator	Component	Number	Cost per unit – currency	Total cost – currency	Source of materials	Material type
SiPM	SiPM (ON-semi MICROFC-60035-SMT-TR)	2	22.45€	44.90€	Mouser Electronics	Other
R1, R2, R3	Resistance 49.9Ω 1% 1/8W 0805	6	0.09	0.54€	Digikey	Other
C1, C2, C3, C4	Capacitor CER 10000pF 50V X7R 0805	8	0.09	0.72€	Digikey	Other
6-pin	6-pin Header	2	0.61	1.21€	Digikey	Other

4.2. Bill-of-material custom PCB

The Bill of Materials of the ADC board and the Raspberry Pi adaptor can be found at OSF

5. Build instructions

5.1. Scintillator paint mixing

1.1 part Kraton D1161 is dissolved in 10 parts White Spirit by mass using a magnetic stirrer or by hand. The dissolving process might take a few hours and can be sped up by gently warming. Using a fume-hood or a well-ventilated area is necessary.

2.When the Kraton is completely dissolved, BN and ZnS:Ag powders are added, see Fig. 2a. The proportions used are 2:8:1 by mass BN:ZnS(Ag):Kraton (All mass proportions are 2BN: 8ZnS(Ag): 1Kraton: 10White Spirit). A stirrer or a spoon is recommended to roughly mix the powders with the Kraton mixture by hand, see Fig. 2b. More white spirit can be added to reduce the viscosity of the liquid as it will evaporate while drying later.

3.To achieve a more homogeneous mixture and increase scintillation efficiency, the mixture is mixed with a blender for 5 to 10 min until all visible lumps are removed and a homogeneous white mixture is achieved, see Fig. 2c.

5.2. Application of scintillator paint

4.For each detector two strips of Mylar of the desired dimensions are cut, see Fig. 3a. An extra margin is included for the tape, this is cut off in the final step. For a total surface area of 0.5m^2 approximately 1L of paint is needed.

5.The first layer is applied with a small paint roller with light pressure, see Fig. 3b. The first layer is applied in one go. Rolling the paint roller over wet paint causes the paint to be absorbed by the paint roller again.

6.The layer is dried before adding another layer in the same manner as in the previous step, see Fig. 3c. The direction of painting is changed each time to get a more homogeneous layer. This step is repeated until ten layers are applied. This will make a total layer thickness of roughly 250 um.
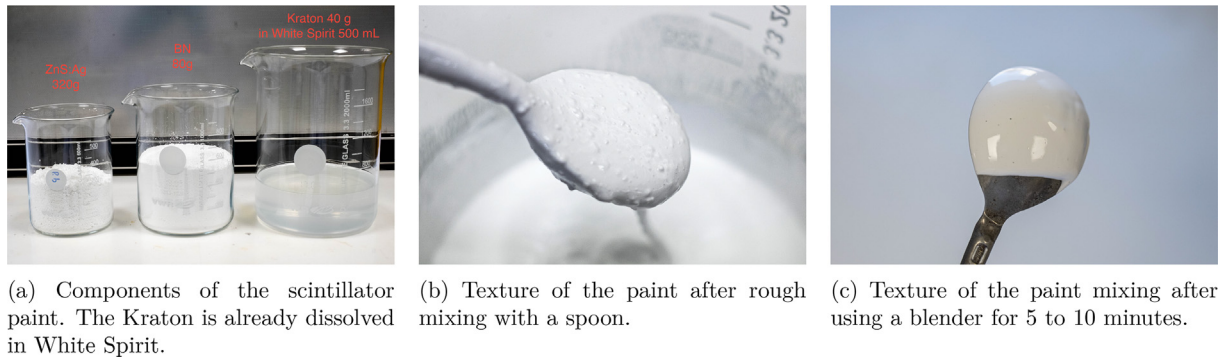
(a) Components of the scintillator paint. The Kraton is already dissolved in White Spirit.

(b) Texture of the paint after rough mixing with a spoon.

(c) Texture of the paint mixing after using a blender for 5 to 10 minutes.

Fig. 2. Scintillator paint mixing.

(a) An example of a small Mylar strip to be painted

(b) Application of the first layer

(c) Adding new layers

(d) Application of the first layer of PVA

(e) Surface texture of final result

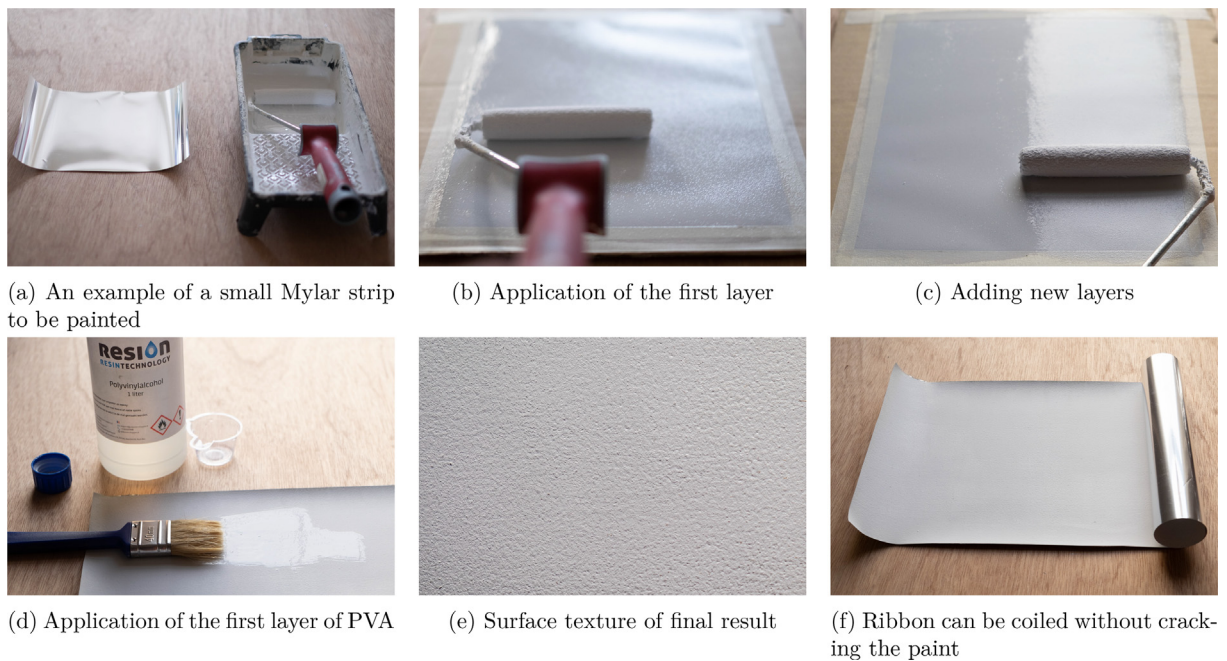(f) Ribbon can be coiled without cracking the paint

Fig. 3. Ribbon-detector Fabrication.

7.After the final layer of paint, two layers of poly-vinyl-alcohol (PVA) are applied at the painted surface with a paint brush, see Fig. 3d. This is to harden the surface of the paint so it will not be damaged by the fibers [1]

8.The surface of the final layer is not flat but textured. This poses no problem as long as the texture and thickness are roughly the same over the entire surface of the ribbon, see Fig. 3e.

9.When the PVA layers are dried, the margins where the ribbons where taped are cut off. The final result are ribbons with one layer of scintillator paint. The paint is flexible and will not crack when the ribbon is rolled up, see Fig. 3f.

5.3. Ribbon-fiber sandwich

10.The ribbons are glued with (spray) glue to a fabric. This fabric is used to prevent the mylar from tearing. The use of synthetic fabrics is discouraged due to the moderating effect it has on neutrons. Here a sheet of unbleached cotton is used. See Fig. 4a

---

[1] Initially, the PVA was applied to prevent alpha radiation created by Radon progeny in the air to reach the scintillator paint layer and create false neutron counts. However, the false neutron count contribution of the Radon progeny is small and will die out mostly within a few hours as the detector is nearly airtight an no new Radon-progeny will enter the detector. [13]

(a) Strips glued on fabric   (b) Cut out and aligned   (c) Mark first line

(d) Sew first line   (e) Mark other lines at desired interval   (f) Positioning the first fiber

(g) Guide the fiber   (h) Final result, margins cut off   (i) Flexible but fibers are kept in place

Fig. 4. Ribbon-detector Fabrication.

11. The ribbons are cut out with 1 cm margin on every side. The two parts are put on top of each other with the painted sides aligned and facing each other. See Fig. 4b
12. At one side, the edge of the mylar is marked with a line, see Fig. 4c
13. The two ribbons are sewn together along the marked line, see Fig. 4d
14. The other lines are marked at the desired fiber interval, Fig. 4e
15. A wavelength shifting fiber is placed along the sew line. Fig. 4f
16. To guide the fiber, a thin tool (for example a screwdriver or a knive) is used. It is placed between the two ribbons just before the presser foot against the fiber such that it pushes the fiber to the left side of the presser foot, see Fig. 4g. The two previous steps are repeated until every fiber is fixed between the ribbons. Afterwards the margins are cut off. See Fig. 4h.
17. The final result is a flexible ribbon that keeps the fibers in place, Fig. 4i.

5.4. SiPM module

18. MDF or plywood is cut by a lasercutter in the shapes as seen in SiPM_module.pdf (3). It can also be done by hand with a handsaw and a drill except for the square window in the center of two of the pieces. This is where the SiPM is positioned and because of the tight fit it makes sure every fiber entering the window will connect to the SiPM.
19. Cable glands are fixed in the circular holes in the centers of the pieces, see Fig. 5a
20. All fiber ends of a detector are put through the cable gland, see 5b. The cable gland is tightened well and the ends of the fiber are cut to make a rough plane of the fiber ends orthogonal to the direction of the fibers, Fig. 5c
21. The plywood piece with the cable glands can be fixed in a vice to facilitate grinding of the fiber end interface. All ends of the fibers are ground with a file or a power-tool at once to achieve a rough flat plane interface, see Fig. 5d
22. Afterwards, all fibers are polished to increase light collection through the fiber ends. This can be done by hand or by a power-tool. When using a power tool make sure a low RPM is used to prevent the fibers from melting, 5e. The fibers can be bundled with a tape to facilitate the polishing.

(a) MDF piece with fiber gland

(b) Bundling of fibers through fiber gland

(c) Cutting

(d) Grinding

(e) Polishing

(f) Final result

(g) SiPM module

(h) SiPM window alignment

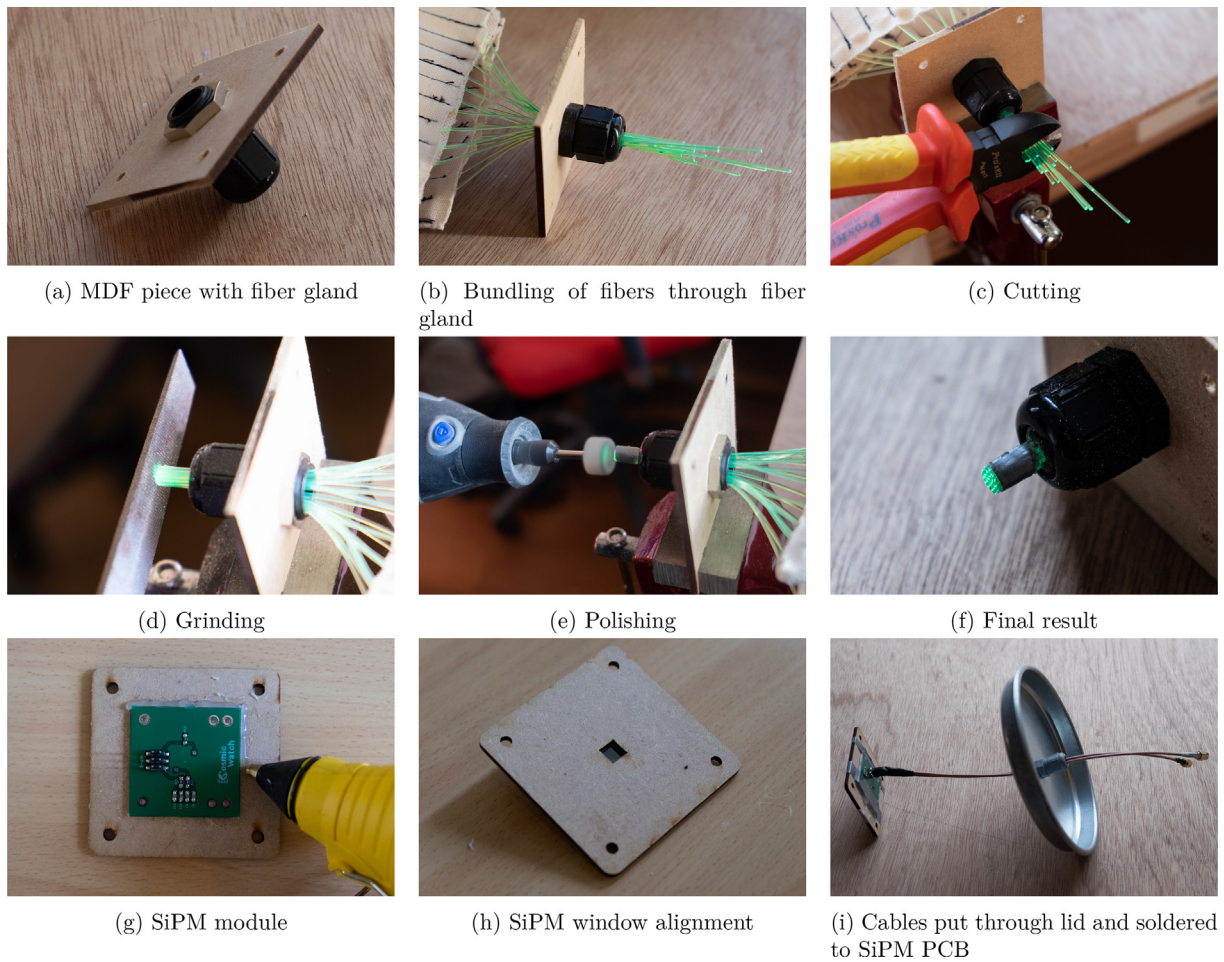(i) Cables put through lid and soldered to SiPM PCB

Fig. 5. SiPM Module.

23. The result, Fig. 5f, is a flat interface of the polished fiber ends.

24. The SiPM PCB is glued or taped (or both) to the other MDF piece of SiPM_module.pdf (3) with the square window such that the SiPM fits in the square window, Fig. 5g and h

25. Two shielded cables are soldered to the 6-pin header at the back of the SiPM module. One of the cable cores is attached to one of the left pins (HV), the core of the other cable is soldered to one of the right pins (SNG). Both grounds go to the center pins, see Fig. 5i

26. A hole is drilled in the lids of the detectors to fit a cable gland. Both cables are put through the cable gland in the lid of the detector. The end of the cables on the other side of the lid are marked HV or SNG. The cable gland is tightened. Fig. 5i.

5.5. Casing installment

27. One end of the aluminium spiro tube is closed off with a spiro lid using a hammer. The HDPE tube is closed off as well with one of the HDPE sheets. The HDPE tube and sheet are glued or taped together. Black isolation tape is used afterwards to cover the seam to ensure it is light tight.

28. The ribbons are coiled or folded up and placed in their casings with the cable gland and the bundle of fibers at the top side. 6a

29. The two pieces of the SiPM module are attached to each other using four bolts and nuts (M4). The nuts are tightened but not forced which will cause damage to the SiPM. See also Fig. 6b

30. The SiPM module is put inside the casing as well, making sure the fiber maximum bending diameter (10 cm) is not exceeded. 6c

31. The open ends of the casing are closed off with their matching lids the same way as in the first step. 6d

32. Each detector is connected to a channel on the oscilloscope or custom PCB. The HV cable is connected to a 29.5 V DC power source. This includes an overvoltage of 4.8 V to the SiPM and is used to increase the gain of the signal, a supplied
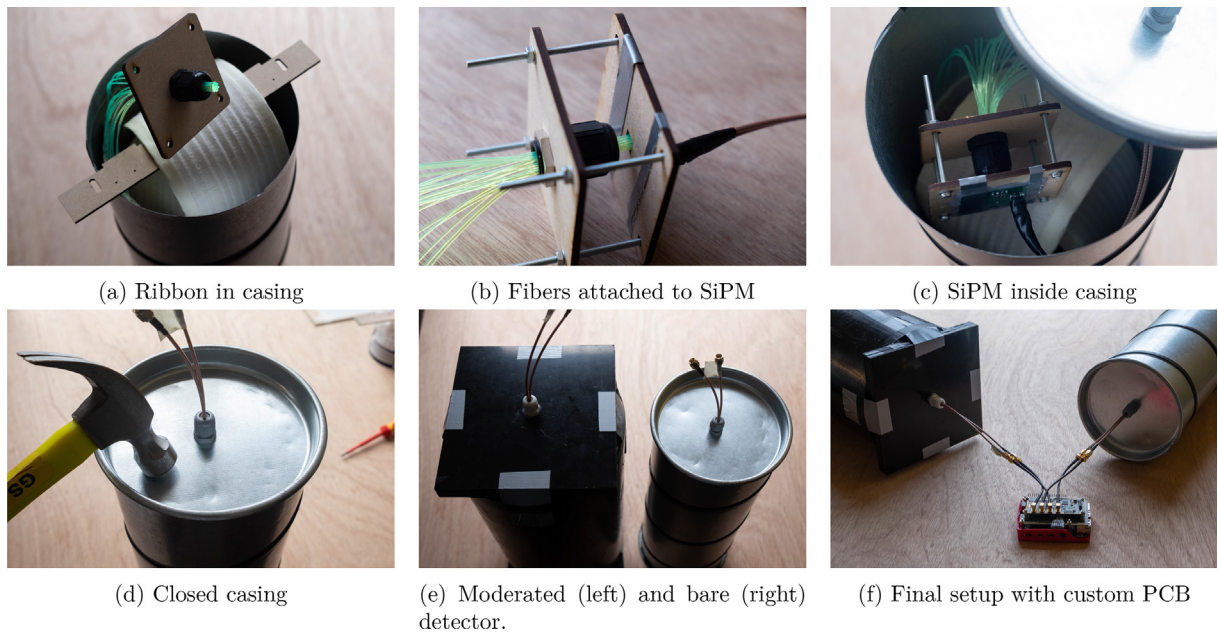
(a) Ribbon in casing

(b) Fibers attached to SiPM

(c) SiPM inside casing

(d) Closed casing

(e) Moderated (left) and bare (right) detector.

(f) Final setup with custom PCB

Fig. 6. Casing installment.

voltage higher than 30 V may cause damage to the SiPM. The SNG cable is connected to the channel of the oscilloscope or the custom PCB, see Fig. 6f.

6. Operation instructions

6.1. Data acquisition

The Picoscope or the custom ADC is connected to the SiPM. A custom-made PCB is preferred to be able to filter and amplify the signal and increase the resolution. Shielded cables are recommended to reduce electromagnetic noise in the signal. The unamplified baseline of the signal should range between −2 mV to + 2 mV if the casing is light-tight. Then a trigger can be set at 6 mV above the baseline value in the unamplified signal. A pulse with a width smaller than 20 ns can be ignored, every other pulse has to be distinguished as either neutron or gamma/noise (6.2) directly or be saved and analysed later.

6.2. Pulse shape discrimination

The ZnS:Ag has been used as a scintillator since the first half of the 20th century because of its scintillation efficiency and its scintillation decay characteristics [7]. However, the opaqueness of ZnS:Ag demands thin layers in order for the scintillation to be visible at the surface. This, in turn, provides an insensitivity to γ-rays because the small thickness of the layers of scintillating material prevent most γ-rays from depositing a large enough portion of their energy to be detected. Still there are scintillation pulses that can be assigned to gamma's which have to be recognised and rejected.

Fortunately, the scintillation decay of a γ-ray excitation is short, 0.1 ns to 10 ns, while the scintillation decay of an α-particle (emitted after neutron absorption by ^{10}B) is longer, up to 10μs [3]. This property opens up a robust way to discriminate between particles using these pulse shapes. An often used method is to define a parameter calculating the fraction of the charge in the tail of the pulse with the charge of the total pulse [9]. The P -parameter is defined as,

$$P = \frac{Q_{long} - Q_{short}}{Q_{long}}$$

(2)

with Q_{long} and Q_{short} the integrated signal of the long part and short part of the signal, respectively. The time gates are set at t_{short} = 400 ns and t_{long} = 4000 ns but can be tweaked for better peak separation (t = 0 corresponds to the trigger).

Due to the decay characteristics of ZnS:Ag, γ-ray pulses will be indicated by low P values while neutrons (i.e. α-particles) are indicated by higher values of P. For every pulse, the P-parameter is determined. Afterwards, a histogram for all pulses categorised by values of the P-parameter is made. After a sufficient number of counts, two clear peaks will be visible in the histogram. The minimum value between the two peaks is the PSD threshold. This step has to be done only once when

installing a setup and can be ignored in later runs when the PSD threshold is already determined. Neutrons are counted by counting pulses for which *P*>PSD threshold.

To determine if the pulse shape discrimination is efficient in distinguishing neutrons from gamma's a Figure-of-Merit can be calculated [15]. The Figure-of-Merit (FoM) is defined as:

$$\text{FoM} = \frac{\langle n \rangle - \langle \gamma \rangle}{FWHM_\gamma + FWHM_n} \tag{3}$$

Here, $\langle n \rangle$, $\langle \gamma \rangle$ and $FWHM_\gamma$, $FWHM_n$ indicate the centroids and full-widths-at-half-maximum of the peaks (or their Gaussian fits), respectively. A FOM value greater than 1.27 is used as a reference parameter to define efficient PSD [20].

6.3. Operation

There are different ways of putting the Python scripts on the Raspberry Pi such as with a SD card or through WiFi. We used WiFi and TeamViewer software (teamviewer.com) to connect from any PC to the Raspberry Pi. The BLOSM_raspi.py is run using, in our case, the Thonny Python IDE (thonny.org).The script will run until stopped.

After a trigger from the ADC, the python script running on the Raspberry Pi (BLOSM_raspi.py) will convert the bytes from the ADC to a string of numbers. It will save the channel, the timestamp (unix), and the entire string of numbers to memory. It will repeat this until it has saved 256 pulses. Then it will save all data in memory to a.csv file, after which it starts to collect pulses again.

All.csv files are zipped and transferred to a PC that runs the analysis script (BLOSM_analyse.py). Running this script will read all.csv files in the directory and turn it into a histogram of both detectors. We did not want to do much processing on the Raspberry Pi, which is why the preference was to download the complete pulse shapes and perform the analysis off-line.This also allows tweaking of the processing parameters.

7. Validation and characterization

The response of both detectors to thermal and fast neutrons is shown in Fig. 8. The first part of the experiment took place in a tube with Cadmium plating of the Reactor Institute Delft, see Fig. 7, to lower the amount of thermal background neutrons and highlight the effect of the neutron source. A significant drop in neutron counts can be seen after the shutdown of the reactor on Jan-29 22:00. The principal part of neutrons emitted by the reactor have thermal energies which are blocked by the Cadmium plating on the tube and cause the lower count rate of the bare detector in comparison with the moderated detector.

The response to thermal neutrons is visible in both detectors. The count rate of the moderated detector is 60% of the count rate of the bare detector for thermal neutrons, with background subtracted. This part of the thermal neutrons is able to penetrate through the HDPE moderator and enter the detector. A solution to this is to surround the HDPE moderator with a piece of thermal neutron shielding material, like boron rubber, to block thermal neutrons and allowing only fast neutrons to be thermalized and reach the detector. This will be part of future design and research.

The response to fast neutrons is also visible in both detectors, although the bare detector response is only 7% in comparison to the moderated detector response, which shows the effectiveness of the moderator. The minimal response of the bare detector is caused by the neutron cross-section of ^{10}B which is small for fast neutrons but still sufficient to absorb a few neutrons.

Under atmospheric background conditions (Delft, the Netherlands), the count-rate of the bare detector ($\sim$6000 per day $\pm$ 1.3%) is slightly higher than the moderated detector ($\sim$4800 per day $\pm$ 1.4%).

The Figures-of-Merit (FoM) can also be seen in Fig. 8 on the right side. The peaks indicating γ-rays (left) and neutrons (right) can be easily distinguished which is also reflected by the FoM values being greater than 1.27.
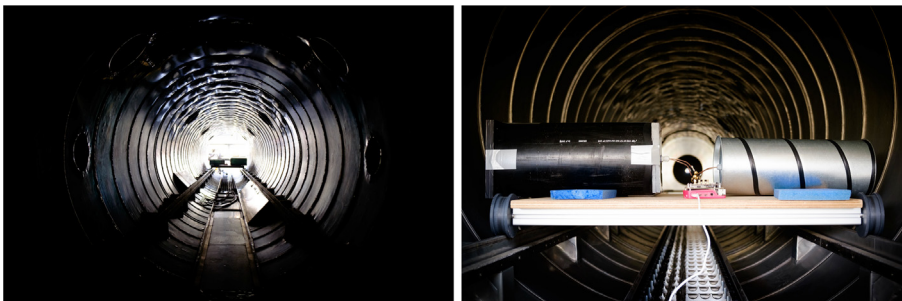

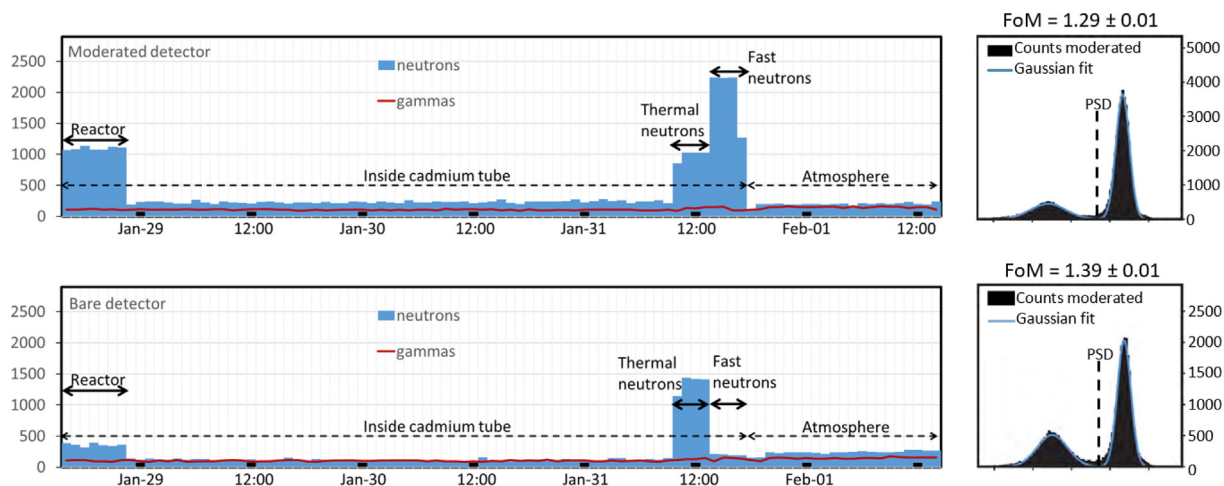**Fig. 7.** Setup BLOSM in Cadmium tube at the Reactor Institute Delft.

Fig. 8. Fast/thermal neutron response experiment at the Reactor Institute Delft. With the exception of the last day of the experiment, the setup was placed inside a Cadmium tube shielding the setup from thermal neutrons. The reactor was running during the first 7 h of the experiment which can be clearly seen in the left plots. The thermal neutrons were produced by a Californium-252 source, moderated by 10 cm polyethylene. The fast neutrons were produced by the same source without the polyethylene moderator. After that, the Cf source was removed and the setup was moved to a place outside the cadmium tube. On the right, histograms of the P-parameter, Eq. (2), of the detectors show clear gamma-peaks (left) as well as clear neutron-peaks (right). The corresponding Figure-of-Merits, Eq. (3), can be seen on top of the plots and are calculated using the Gaussian fit. The indicated PSD value is positioned at the minimum value of the Gaussian fit between the peaks.

In conclusion, the count rate of both detectors is high enough to get a daily count with an error smaller than 1.5% and Pulse Shape Discrimination can be carried out accurately. The moderated detector is able to detect fast neutrons efficiently while it is also sensitive to thermal neutrons. The bare detector can be used to determine the part of the neutron spectrum with thermal energies.

- The mean coefficient of variation is approximately 1.3% for a daily measurement with a count of 6000 neutrons (mean daily atmospheric neutron count for the described setup). The coefficient can vary depending on the count-rate, i.e. the size of the neutron sensitive material, the scintillation efficiency and atmospheric neutron production.
- With a custom PCB + Raspberry Pi setup, the power consumption varies between 4 W and 6 W which can easily be provided by a solar panel to create a standalone setup. If a laptop and Picoscope are used for data acquisition, the power consumption can increase to 60 W to 100 W per detector which makes this setup only suitable for labs or places with a power outlet.
- The setup is made to be constantly operating to monitor the neutron count for long time-spans. The neutron-sensitive material will be affected little by environmental conditions because of the air-tight and light-tight casings. Only temperature changes will influence the electronics, the SiPM will experience more thermal noise peaks at higher temperatures which should be rejected after PSD if done correctly.

7.1. Further work

It should be stressed that we present here only the laboratory validation of the detectors that shows that we can indeed detect and count thermal and fast neutrons. There is still work do be done before this set-up has been tested in the field. In principle, we can measure the ratio between thermal and fast neutrons, which should give an estimation of the soil-moisture content when other neutron-moderating factors in the environment are neglected. These factors, for instance water vapour, vegetation and surface water can be accounted for with corrections which have to be calibrated. Several soil samples have to be taken from the area to determine the initial soil-moisture factor. To correct for water vapour and air pressure each detector should be equipped with a hygrometer and a barometer. The correction factors are well documented in earlier research and their magnitude can be easily determined with known equipment [22]. Given that CRNS has been extensively proven to correlate with large scale soil moisture, not a complete method validation would be needed but some field campaigns that include traditional soil moisture measurements, will be needed to show that the intended use of BLOSM is feasible in the field.

CRediT authorship contribution statement

Edward Amelrooij: Methodology, Validation, Formal-analysis, Investigation, Data-curation, Writing-original-draft, Visualization. **Nick de Giesen:** Conceptualization, Writing-review-editing, Supervision, Project-administration, Funding-

acquisition. **Jeroen Plomp:** Conceptualization, Investigation, Resources, Writing-review-editing. **Michel Thijs:** Investigation, Resources, Writing-review-editing. **Tomáš Fico:** Methodology, Software, Resources.

Declaration of Competing Interest

Acknowledgements

References

[1] Spencer N. Axani, Katarzyna Frankiewicz, Janet M. Conrad, The cosmicwatch desktop muon detector: a self-contained, pocket sized particle detector, J. Instrumentation, 13(03):P03019, 2018..
[2] J.P. Bell, Neutron probe practice (1987).
[3] L.D. Hendrick, R.D. Edge, Cosmic-ray neutrons near the earth, Phys. Rev. 145 (4) (1966) 1023.
[4] J.B. Birks, The Theory and Practice of Scintillation Counting, Pergamon Press, 1964.
[5] C. Jackson, L. Wall, K. O'Neill, B. McGarvey, D. Herbert, Ultra-low noise and exceptional uniformity of SensL C-series SiPM sensors. Optical Components Mater. XII, March 2015..
[6] Glenn F. Knoll. Radiation detection and measurement. John Wiley, Hoboken, N.J, 4th ed edition, 2010. OCLC: ocn612350364..
[7] P.G. Koontz, G.R. Keepin, J.E. Ashley, ZnS(Ag) Phosphor Mixtures for Neutron Scintillation Counting. The Review of Scientific Instruments, page 6, June 1954..
[8] Richard T. Kouzes, Azaree T. Lintereur, Edward R. Siciliano, Progress in alternative neutron detection to address the helium-3 shortage, Nucl. Instrum. Methods Phys. Res. Section A: Accelerators, Spectrometers, Detectors and Associated Equipment 784 (June 2015) 172–175.
[9] A. Kozlov, D. Chernyak, A large area detector for thermal neutron flux measurements at the KamLAND site, Nucl. Instrum. Methods Phys. Res. Section A: Accelerators, Spectrometers, Detectors and Associated Equipment 903 (September 2018) 162–169.
[10] Kuraray. Kuraray Wavelength Shifting Fibers Specifications..
[11] Edward James Marsden, Large area thermal neutron detectors for security applications. phd, University of Sheffield, 2013.
[12] John McMillan, Edward Marsden, Neutron Detectors for Security Applications, Proc. Sci. 113(VERTEX 2010) (2011) 2010:031.
[13] National Institute of Standards and Technology. Radium-226 Decay Chain, 1927..
[14] A. Osovizky, Kevin Pritchard, Y. Yehuda-Zada, Jeffrey Ziegler, E. Binkley, Peter Tsai, Alan Thompson, Nancy Hadad, M. Jackson, C. Hurlbut, et al., Design of an ultrathin cold neutron detector, Nucl. Instrum. Methods Phys. Res. Section A: Accelerators, Spectrometers, Detectors and Associated Equipment, 893:1–9, 2018..
[15] I.A. Pawełczak, A.M. Glenn, H.P. Martinez, M.L. Carman, N.P. Zaitseva, S.A. Payne, Boron-loaded plastic scintillator with neutron-pulse shape discrimination capability, Nucl. Instrum. Methods Phys. Res. Section A: Accelerators, Spectrometers, Detectors and Associated Equipment 751 (July 2014) 62–69.
[16] Varley F. Sears, Neutron scattering lengths and cross sections, Neutron News 3 (3) (January 1992) 26–37.
[17] R. Stedman, Scintillator for Thermal Neutrons using Li^6 F and ZnS (Ag), Rev. Sci. Instrum. 31 (10) (October 1960), 1156–1156.
[18] Luca Stevanato, Gabriele Baroni, Yafit Cohen, Cristiano Lino Fontana, Simone Gatto, Marcello Lunardon, Francesco Marinello, Sandra Moretto, Luca Morselli. A Novel Cosmic-Ray Neutron Sensor for Soil Moisture Estimation over Large Areas. Agriculture, 9(9):202, September 2019..
[19] C.W.E van Eijk, A Bessière, and P Dorenbos. Inorganic thermal-neutron scintillators. Nucl. Instrum. Methods Phys. Res. Section A: Accelerators, Spectrometers, Detectors and Associated Equipment, 529(1–3), 260–267, August 2004..
[20] Natalia Zaitseva, Benjamin L. Rupert, Iwona Pawełczak, Andrew Glenn, H. Paul Martinez, Leslie Carman, Michelle Faust, Nerine Cherepy, Stephen Payne, Plastic scintillators with efficient neutron/gamma pulse shape discrimination, Nucl. Instrum. Methods Phys. Res. Section A: Accelerators, Spectrometers, Detectors and Associated Equipment, 668:88–93, March 2012..
[21] James F. Ziegler, Terrestrial cosmic rays, IBM J. Res. Develop. 40 (1) (1996) 19–39.
[22] M. Zreda, W.J. Shuttleworth, X. Zeng, C. Zweck, D. Desilets, T. Franz, R. Rosolem, COSMOS: the COsmic-ray Soil Moisture Observing System, Hydrol. Earth Syst. Sci. 16 (11) (November 2012) 4079–4099.